52-003

UNITED STATES
NUCLEAR REGULATORY COMMISSION
WASHINGTON, D.C. 20555-0001

Novmeber 7, 1996

Mr. Nicholas J. Liparulo, Manager
Nuclear Safety and Regulatory Activities
Nuclear and Advanced Technology Division
Westinghouse Electric Corporation
P.O. Box 355
Pittsburgh, Pennsylvania 15230

SUBJECT: FOLLOWON QUESTIONS REGARDING REACTOR VESSEL INTEGRITY DURING SEVERE ACCIDENT CORE MELTS

Dear Mr. Liparulo:

In a May 22, 1996, letter the staff transmitted two reports to Westinghouse concerning reactor vessel integrity during severe accident core melts. Enclosure 1 to this letter provided Idaho National Engineering Laboratory (INEL) comments and questions on the application of the Department of Energy (DOE) report DOE/ID-10460, "In-Vessel Coolability and Retention of a Core Melt," dated July 1995. This enclosure was provided to Westinghouse for information and consideration, and was to serve as the basis for future discussions on the topic.

A teleconference was held with Westinghouse, INEL, Dr. Theofanous, DOE, and members of the staff on October 25, 1996, to discuss Enclosure 1 of the May 22, 1996, letter. Unfortunately, this teleconference did not prove productive in addressing the concerns identified in the letter. Therefore, the staff has decided to reissue Enclosure 1 of the May 22, 1996, letter as requests for additional information (RAIs). Please note that the only difference between Enclosure 1 of the May 22, 1996, letter and the Enclosure to this letter is that RAI numbers have been assigned to the INEL comments and questions.

Although this letter is being reissued unchanged except as noted above there are several typographical errors that remain in the enclosure. They are listed here to ensure that you are aware of the problems with the letter. The errors include the following:

- Figure 2 and 3 on page 3 should be labeled figure 1 and 2 respectively.
- The last sentence of the first paragraph on page 12 should have the parameters and the temperatures changed and should read as follows: "Thus the radiative sink temperature, $T_{s,i}$, of approximately 960 K (Figure Q.10) and the melt surface temperature, $T_{l,o}$, of approximately 1710 K would be inappropriate for such a configuration."
- The third paragraph under Finite Element Analysis on page 14 should have the first occurrence of 2.5 cm changed to 5.0 cm and should read as follows: "... Figure 4.6 also indicates that the wall thickness is 5.0 cm;...".

DF03
1/1

If you have any questions regarding this matter, you can contact me at (301) 415-1132.

Sincerely,

original signed by:

Joseph M. Sebrosky, Project Manager
Standardization Project Directorate
Division of Reactor Program Management
Office of Nuclear Reactor Regulation

Docket No. 52-003

Enclosure: As stated

cc w/enclosure:
See next page

DISTRIBUTION:

Docket File	PDST R/F	JSebrosky
PUBLIC	BPalla, 0-8 H7	JMonninger, 0-8 H7
FEltawila. T-10 G6	FOdar, T-10 G6	CBerlinger, 0-8 H7
JKudrick, 0-8 H7	GHolahan, 0-8 E2	EJordan, T-4 D18

DISTRIBUTION w/o enclosure:

TMartin	DMatthews	TQuay
TKenyon	DJackson	WHuffman
WDean, 0-17 G21	JMoore, 0-15 B18	ABehbahani, T-10 K8
ACRS (11)	ARubin, T-10 K8	YChen, T-10 K8
SBasu, T-10 K8		

DOCUMENT NAME: A:IVR SCSB.RAI (9J AP600 DISK)
To receive a copy of this document, indicate in the box: "C" = Copy without attachment/enclosure "E" = Copy with attachment/enclosure "N" = No copy

OFFICE	PM:PDST:DRPM		SCSB:DSSA		D:PDST:DRPM					
NAME	JSebrosky:sg		Jkudrick		TRQuay					
DATE	11/7/96		11/7/96		11/7/96					

OFFICIAL RECORD COPY

Mr. Nicholas J. Liparulo
Westinghouse Electric Corporation

Docket No. 52-003
AP600

cc: Mr. B. A. McIntyre
Advanced Plant Safety & Licensing
Westinghouse Electric Corporation
Energy Systems Business Unit
P.O. Box 355
Pittsburgh, PA 15230

Mr. John C. Butler
Advanced Plant Safety & Licensing
Westinghouse Electric Corporation
Energy Systems Business Unit
Box 355
Pittsburgh, PA 15230

Mr. M. D. Beaumont
Nuclear and Advanced Technology Division
Westinghouse Electric Corporation
One Montrose Metro
11921 Rockville Pike
Suite 350
Rockville, MD 20852

Mr. Sterling Franks
U.S. Department of Energy
NE-50
19901 Germantown Road
Germantown, MD 20874

Mr. S. M. Modro
Nuclear Systems Analysis Technologies
Lockheed Idaho Technologies Company
Post Office Box 1625
Idaho Falls ID 83415

Mr. Frank A. Ross
U.S. Department of Energy, NE-42
Office of LWR Safety and Technology
19901 Germantown Road
Germantown, MD 20874

Mr. Ronald Simard, Director
Advanced Reactor Programs
Nuclear Energy Institute
1776 Eye Street, N.W.
Suite 300
Washington, DC 20006-3706

Ms. Lynn Connor
Doc-Search Associates
Post Office Box 34
Cabin John, MD 20818

Mr. James E. Quinn, Projects Manager
LMR and SBWR Programs
GE Nuclear Energy
175 Curtner Avenue, M/C 165
San Jose, CA 95125

Mr. Robert H. Buchholz
GE Nuclear Energy
175 Curtner Avenue, MC-781
San Jose, CA 95125

Barton Z. Cowan, Esq.
Eckert Seamans Cherin & Mellott
600 Grant Street 42nd Floor
Pittsburgh, PA 15219

Mr. Ed Rodwell, Manager
PWR Design Certification
Electric Power Research Institute
3412 Hillview Avenue
Palo Alto, CA 94303

Mr. Charles Thompson, Nuclear Engineer
AP600 Certification
NE-50
19901 Germantown Road
Germantown, MD 20874

INEL Comments and Questions about DOE/ID-10460

INEL's review indicates that Reference 1 applied the approach shown below to demonstrate vessel integrity for cases with complete RCS depressurization and ex-vessel cavity flooding. As indicated in this figure, the authors must prove two assertions in order to insure vessel integrity:

- For all heat fluxes at or below the CHF, the corresponding minimum vessel wall thicknesses are sufficient that the vessel remains intact.
- Heat fluxes to the lower head always remain below CHF.

As indicated in the figure below, various types of information (analyses, experiments, and assumptions) were used to support each assertion. Starting at the far right of this figure, the authors used CHF data from the ULPU tests to estimate minimum vessel thickness for the structural analyses and provide bounding heat fluxes for the thermal analyses. For the minimum vessel wall thicknesses, the authors performed structural calculations to demonstrate that the vessel remains intact if heat fluxes are at or below the CHF (Assertion 1). Thermal analyses are performed for two bounding configurations to determine maximum possible heat fluxes. These heat fluxes (and associated uncertainties) are shown to be below the CHF values (Assertion 2). Hence, the authors concluded that the vessel remained intact for cases with complete RCS depressurization and ex-vessel cooling. The authors relied on peer reviewer concurrence to validate the adequacy of the information supporting each assertion.

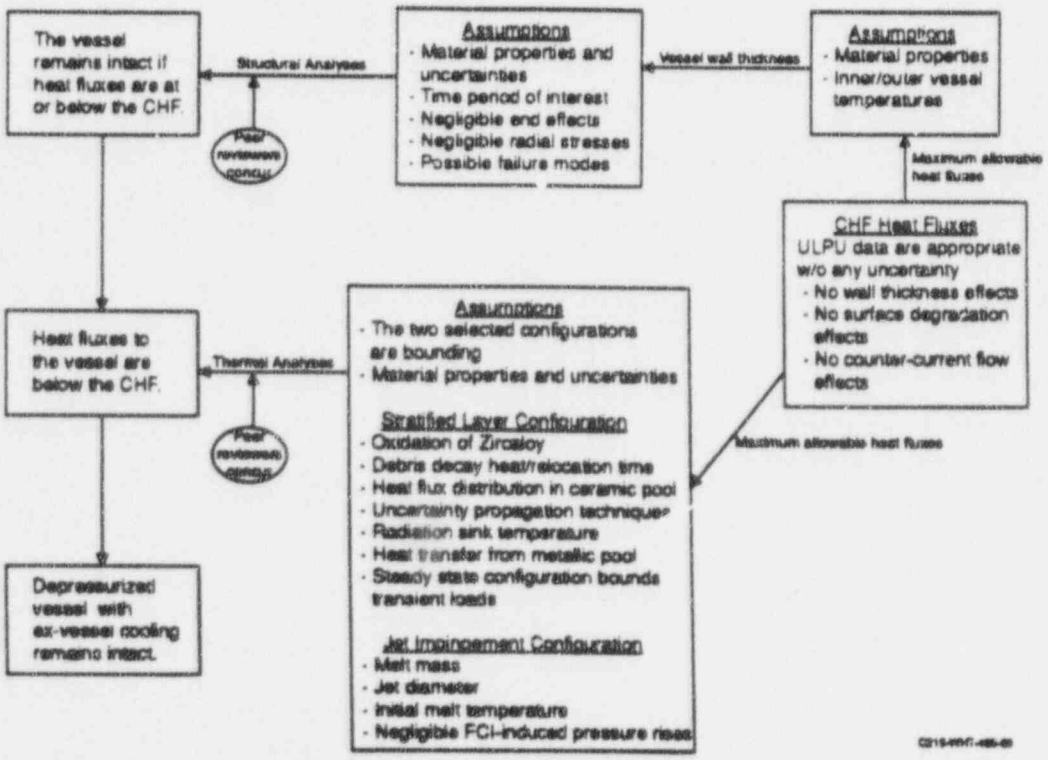

DOE/ID-10460 strategy for demonstrating AP600 In-Vessel Retention

In helping NRC evaluate the conclusions from Reference 1, INEL is reviewing all of the assumptions, experimental data, and analyses listed above. This paper contains preliminary questions about the assumptions, experimental data, and analyses used to support each assertion.

Enclosure 1

Thermal Analyses

Uncertainties

480.440 Uncertainty estimates provided in Reference 1 are incomplete and as such, tend to understate overall uncertainties in the thermal loads. Please revise the main Section 7.2 calculations comprehensively considering appropriate values for the following uncertainties:

Material properties. As discussed below, Table 7.1 implies that Section 7 calculations assumed uncertainty distributions that were inconsistent with those presented in Appendix L. Furthermore, uncertainties in many material properties (melting temperatures, density, specific heat, and emissivity) appear to have been neglected.

Natural convection heat transfer correlation (upward, downward, and local correlations). Natural convection correlations contain uncertainties associated with experimental conditions and uncertainties introduced in fitting a natural convection correlation to the data. As discussed below, there are also uncertainties associated with heat transfer because of phenomena, such as transient phenomena and vapor transport effects.

Decay power curve uncertainties. There are non-negligible uncertainties associated with decay power curves. Furthermore, as discussed below, it appears that uncertainty distributions for pool power density are too small.

Metal layer heat transfer. There is uncertainty associated with the assumed minimum thickness of the layer and the assumed heat transfer correlations. Furthermore, there is the potential for oxidation to produce significant heat sources in the metal and to reduce upward heat losses from upper surface of the metal layer.

480.441 As discussed below, there are other debris configurations that may produce more severe thermal loads to the vessel wall. Please provide appropriate probabilities for various postulated endstates.

Molten Pool Natural Convection Heat Transfer Assumptions

480.442 Figures 1 and 2 compare several natural convection heat transfer correlations developed from various experimental and analytical studies. In these figures, correlations are plotted over the range of Rayleigh numbers for which they were developed. As shown in these figures, there is considerable scatter between various correlations. Comparing the experimentally-developed, Kymalainen and Theofanous correlations, one can see that the ratio of upward to downward heat transfer is lower for the Theofanous data in the higher Rayleigh number range. Thus, an analyses assuming the Theofanous correlations (based on mini-ACOPO data) will predict less heat being transferred to the metal layer above the ceramic debris and reduced heat fluxes from the metal layer to the wall. This trend is demonstrated in Figure 7.15, which investigates a sensitivity in which the Mayinger correlation was substituted for the mini-ACOPO Theofanous correlation (the Mayinger correlation is lower than the Theofanous correlation for pool Rayleigh numbers of 10^{15}). Larger differences exist between the Theofanous and Kymalainen correlations than the Mayinger and Theofanous correlation for pool Rayleigh numbers at 10^{15}. In their response to Dr. Schmidt, the authors state that these differences are due to the shape of the lower boundary. However, this emphasis on geometry yields the author's data as the only data applicable to these tests. Furthermore, mini-ACOPO data do not agree with other hemispherical correlations at low Rayleigh numbers. Please perform a sensitivity study based on the Kymalainen data.

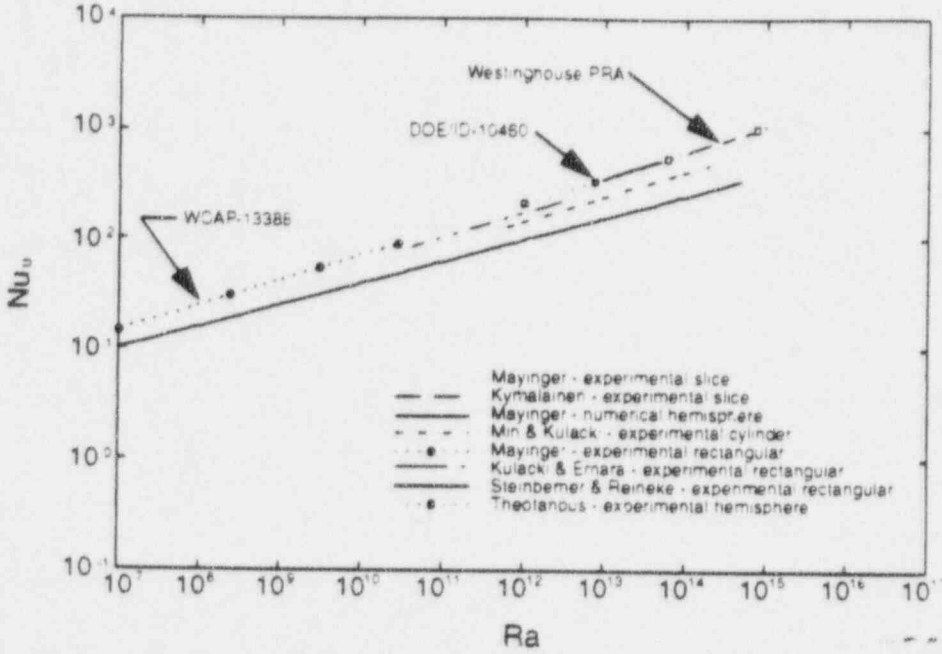

Figure 2. Comparison of correlations for predicting upward heat transfer.

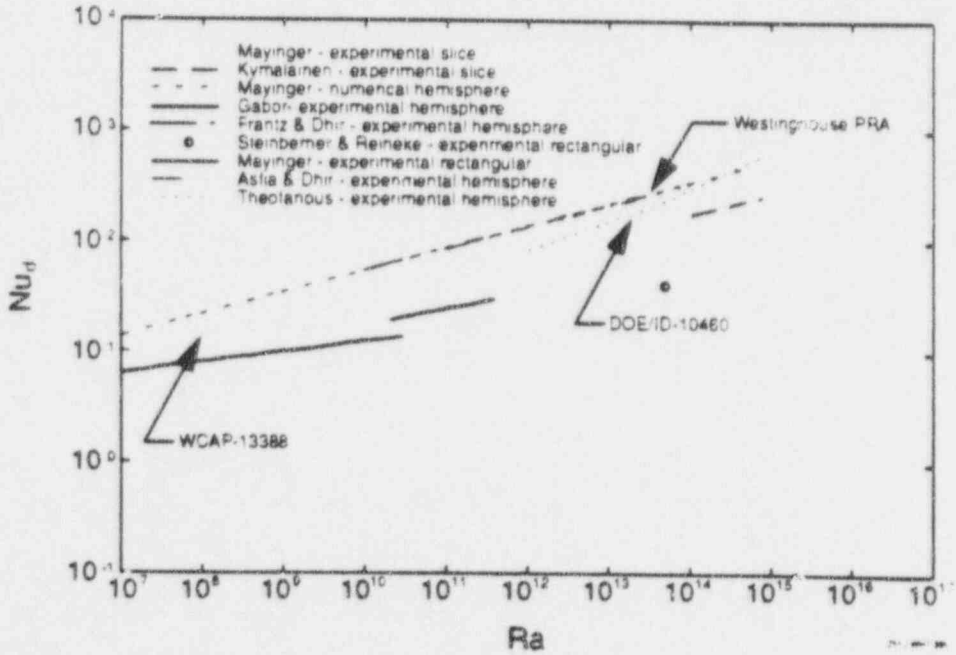

Figure 3. Comparison of correlations for predicting downward heat transfer.

480.443 Figure 5.8 compares ratios of local to average Nusselt numbers from several numerical and experimental studies. As noted in the caption, these curves have been area averaged to correct for differences between tests run in slice and hemispherical geometries. As discussed during the March 21, 1996, NRC/DOE/Westinghouse meeting, this correction was performed by dividing the ratio, $Nu_{x-d}/Nu_{d-slice}$, with the following ratio

$$\frac{\overline{Nu_{d-hem}}}{\overline{Nu_{d-slice}}} = \frac{\int \frac{Nu_{x-d}}{\overline{Nu_{d-slice}}} dA_{hem}}{\int dA_{hem}} = \frac{\int \frac{Nu_{x-d}}{\overline{Nu_{d-slice}}} (2\pi R)\, dR}{2\pi R^2} \qquad (1)$$

Please clarify how this equation was applied to obtain the Figure 5.8 Mayinger curve. Assuming the Mayinger (1985) curve is based on information from Mayinger (1975)[a] and Jahn and Reineke (1974), INEL obtained the curve shown in Figure 3. Note that the peak local value (at 90 degrees) is lower than either the mini-ACOPO curve or the Mayinger (1985) curve shown in Figure 5.8. Please discuss the equations used to obtain the Figure 5.8 Mayinger (1985) curve and include the Kymalainen COPO local values in Figure 5.8.

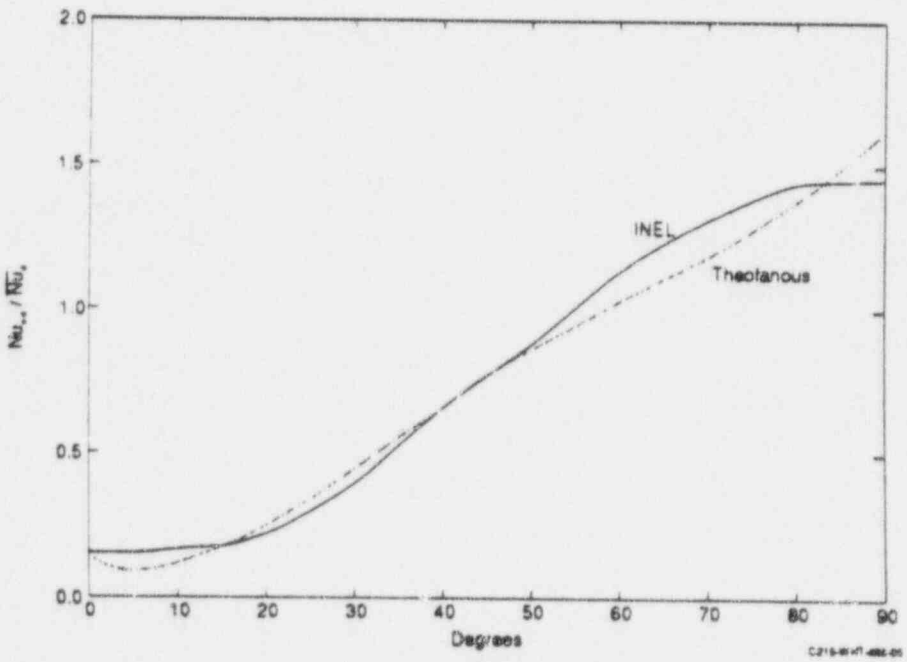

Figure 3. Comparison of area corrected localized Mayinger data.

480.444 The potential for higher transient thermal loads (than those at steady state) at lower positions on the lower head is acknowledged on p. 5-10. As the authors discussed in their responses to Drs. Seghal and Schmidt, an addendum was included in Appendix D that discusses mini-ACOPO transient data to provide insights about the development, with time, of heat flux distributions. Data presented in this addendum were taken from tests in which the time required for steady-state conditions to occur was minimized.

---

[a] The DOE/ID-10460 reference list did not contain a Mayinger (1985) entry. Hence, it was assumed that the Mayinger (1985) curve represents the Mayinger (1975) data.

The authors and Dr. Schmidt exchanged several comments regarding whether transient natural convection relates to the boundary layer or the bulk pool time constant. The authors note that the boundary layer time constant is on the order of 2 minutes. However, a bulk pool time constant corresponding to a molten pool in the AP600 lower head would be considerably longer. In Min and Kulacki,[2] the following relationship was developed based on experimental data for estimating the time required for steady-state behavior.

$$t_{ss} = \frac{L^2}{\alpha} 23.34 \, (\Delta Ra^{-0.223}) \qquad (2)$$

Assuming the material properties in Appendix L and Table 7.2, this relationship suggests that transient behavior may last as long as 10 hours. In Appendix V, Dr. Schmidt identifies this point as an open item and the authors state that they anticipate that ACOPO data will resolve any questions about the characteristic time for steady state conditions.

Data in the addendum to Appendix D suggest how transient heat fluxes may vary as a function of time. Data from several tests (A5, A10, and A6) suggest that at later times, the ratios of the local to average Nusselt numbers become larger at locations near the 90 degree location and that ratios of local to average Nusselt numbers become smaller near the 10 degree location (no data were plotted for the 0 degree location). Hence, these data support the assertion that heat loads to the vessel at lower angles (where the CHF values are lower) may be higher during transient time periods.

To resolve questions related to transient behavior, please provide the following:

-An explanation of the behavior observed at the 40 degree location in runs A3, A4, and A6.

-The ACOPO data to resolve Dr. Schmidt's comments

-A sensitivity study using a distribution that bounds the flatter flux shape distributions that may occur during transient stages of natural convection.

480.445 In Dr. Tuomisto's comments, he noted that the presence of materials with lower vaporization temperatures in the ceramic pool could increase heat transfer rates from the ceramic pool to the metal layer. In Appendix O, the authors responded that there is no mechanism for entrapping significant quantities of steel below superheated oxidic melt. However, there is a potential for superheated steel and control materials to be mixed within the molten pool. The presence of such lower vaporization temperature materials is supported by voids measured in examinations of debris from the TMI-2 vessel and the LOFT fuel damage tests (porosities of at least 20%). Using correlations based on experiments performed by Greene, et al.,[3] INEL performed calculations to estimate the impact of vapor on heat transfer to the side walls.[4] As shown in Figure 4, boiling significantly increases heat transfer for pool Rayleigh numbers of interest. Information in Reference 4 indicates that upward heat transfer experiences a similar increase because of vapor transport. Have calculations been performed to quantify the time required for these materials to vaporize from a ceramic pool? Please provide calculations assessing the impact of vapor transport effects on the margins to CHF.

Molten Metal Layer Heat Transfer

480.446 Please provide the following Chapter 5 Addendum information:

-Identify the two-dimensional heat transfer model used for these calculations.

-Clarify how the vessel dimensions and heat fluxes shown in Figure 5.15 were derived.

-Clarify the impact of applying results from a vertical, flat plate analyses to a structure that is angled (the Figure 5.15 diagram should be at least 70 degrees as indicated in Figure 4.8).

-Explain why heat fluxes are higher within the unmelted vessel steel in Figure 5.16 (heat fluxes of nearly 1600 kW/m^2 are predicted within the vessel, but not on the surface).

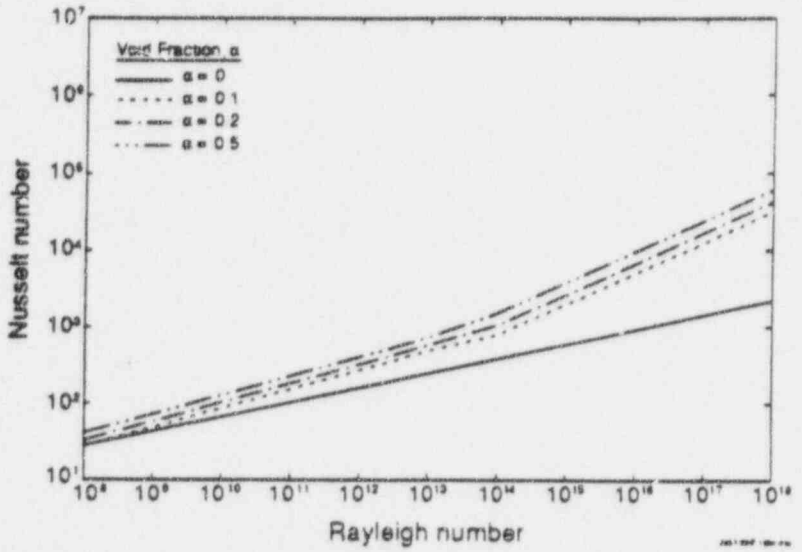

Figure 4. Impact of boiling on heat transfer from a molten pool.

480.447 Several references discuss experiments that have been performed with an internally heated fluid layer below a second unheated, immiscible fluid layer.

- G. Fieg, "Experimental Investigations of Heat Transfer Characteristics in Liquid Layers with Internal Heat Sources," *Proceedings of the ANS-ENS International Meeting on Fast Reactor Safety and Related Physics*," Chicago, USERDA Report CONF-761001-P4, 1976, pp. 2047-2055.
- R. Schramm and H. H. Reineke, "Natural Convection in a Horizontal Layer of two Different Fluids with Internal Heat Sources," *Proceedings of the Sixth International Heat Transfer Conference, Toronto, Canada*, Vol. 2, Paper NC-20, 1976, pp. 299-304.
- F. A. Kulacki, A. A. Emara, J. H. Min, and A-T. Nguyen, "Experimental Studies of Steady and Transient Natural Convection with Internal Heat Sources in Enclosed Cavities," *Proceedings of the Fourth Water Reactor Safety Research Meeting, Gaithersburg, MD*, 1976.
- F. A. Kulacki and A-T Nguyen, *Hydrodynamic Instability and Thermal Convection in a Horizontal Layer of Two Immiscible Fluids with Internal Heat Generation*, NUREG/CR-2619R3, 1980.

Correlations developed from Fieg and Kulacki, et al. for upward heat transfer are compared with the Globe-Dropkin correlation in Figure 5. As shown in this figure, the Globe-Dropkin correlation applied in Reference 1 predicts higher upward heat losses from the metal layer. Assess the impact on results if the Fieg and Kulacki data were used instead of the Globe-Dropkin correlation.

Material Properties

480.448 A liquidus temperature of 1573 K is assigned to the metallic layer on p. 5-2 with reference to Figure 6.1. It appears that the specified temperature corresponds to a Zr mole fraction of ~0.1. It is not clear why other temperatures (corresponding to other possible Zr mole fractions) are not considered. Appendix P indicates that 1600 K is the lowest possible temperature of any Fe-Zr eutectic in which iron is the dominant component. However, it is not clear

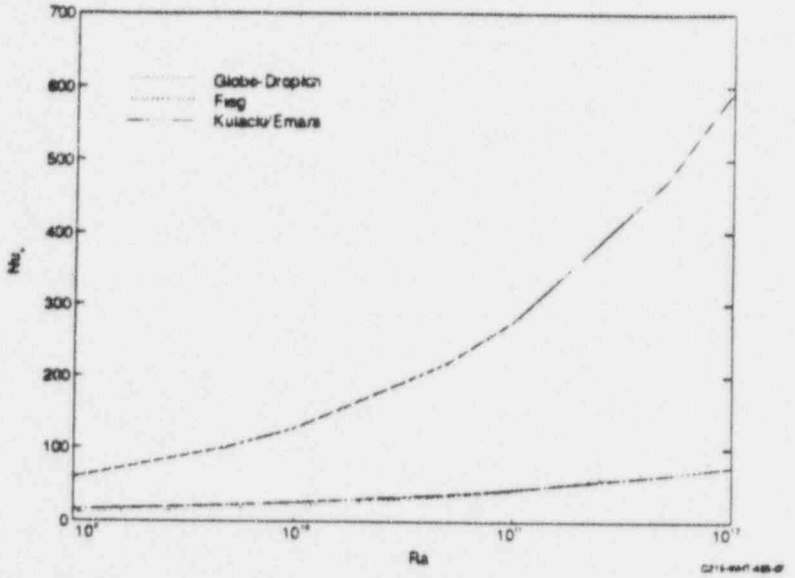

Figure 5. Comparison of correlations for predicting upward heat transfer from the metal layer.

that iron is necessarily the dominant component. Best-estimate SCDAP/RELAP5 calculations have been completed for a scenario similar to the one considered in Reference 1. Results from those calculations indicate that the mole fraction of unoxidized Zr (before lower core plate melting) could approach 50%. Higher Zr mole fractions may be possible in some locations if the metallic melt is not well mixed. In their response to Olander, the authors noted that "the composition cannot be specified with any degree of accuracy." However, no sensitivities were performed to consider the impact of this temperature.

For example, it appears that Figure 4.1 was obtained by using the best estimate values for critical heat flux (Figure 3.3), vessel wall thermal conductivity (32.0 W/K-m per Table 7.1), and iron-zirconium liquidus temperature (Figure 6.1). If one considers the uncertainties in the vessel thermal conductivity (± 10% according to Appendix L) and the iron-zirconium liquidus temperature (variations in the mole fraction of zirconium may lead to liquidus temperatures between 1201 and 1948 K), the CHF-limited wall thickness could be as small as 1.5 cm (compared to the 2.5 cm shown at 90 degrees in Figure 4.1). If one were to consider the uncertainties estimated by others for similar experiments (± 20%),[5] the CHF-limited wall thickness would be reduced even further as shown in Figure 6. As discussed in the structural analyses comments, this thickness (and other uncertainties related to the structural analyses presented in Section 4) reduces the robustness of Section 4 conclusions, and the finite element calculations should be revised using an appropriate vessel wall thickness

480.449 Page 7-1 indicates that values for thermophysical properties and their 2σ values are listed in Table 7-1 based on information in Appendix L. However, Table 7-1 lists single values for many of the properties in Table 7.1 (e.g., density, specific heat, emissivity, and melting point). With the exception of viscosity, most of the ceramic pool properties listed in Table 7.1 are not shown to vary as a function of temperature. Furthermore, there is no indication that these properties were varied with temperature in the calculations for estimating the pool Rayleigh numbers. Please discuss how ceramic pool temperature-dependent properties and debris and vessel material property uncertainties were considered in these calculations.

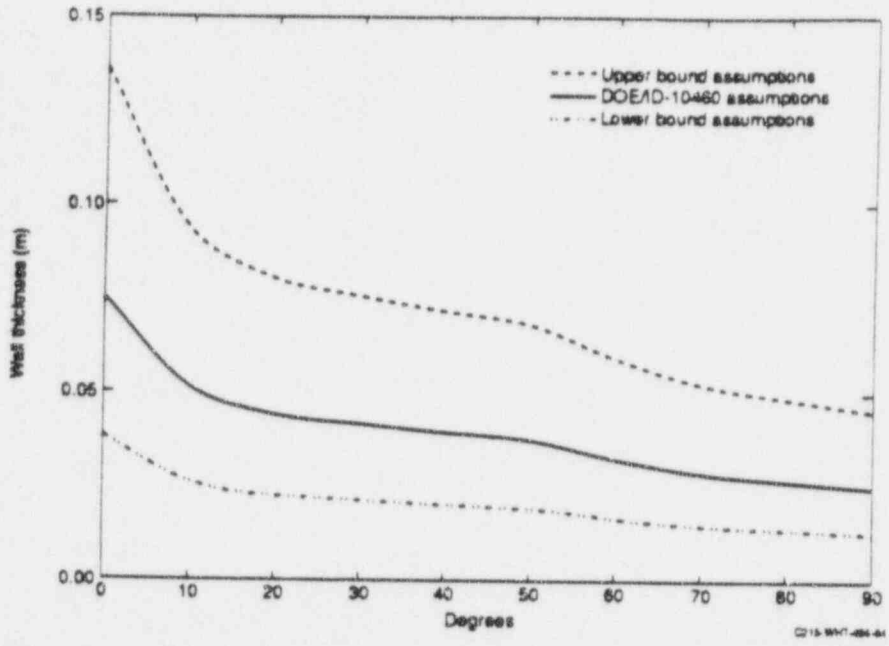

Figure 6. Possible CHF-limited vessel wall thicknesses (Upper bound assumptions correspond to maximum vessel melting temperature and reduced CHF values; Lower bound assumptions correspond to minimum vessel melting temperatures and maximum CHF values).

480.450 Table 7.1 suggests that many of the Appendix L material property uncertainty estimates were neglected in estimating the overall uncertainties in the wall heat fluxes. Uncertainties in melting temperatures, density, specific heat, and emissivity were not included in the values given in Table 7-1 even though there are uncertainties in these parameters associated with composition and temperature as noted in Appendix L. In addition, the uncertainty estimates provided for the effective thermal conductivity of the ceramic crust are not consistent with those presented in Appendix L. Table L-3 shows that the thermal conductivity of the crust can vary between 5.6 $\pm$ 1.1 to 2.0 $\pm$ 0.3 W/mK, depending upon the composition in the crust, yet Table 7.1 used 2.8 $\pm$ 0.4 W/mK. Appendix L material property uncertainties do not include uncertainties associated with prototypic crusts such as the influence of other materials in the crust or porosity of the crust. For example, the thermal conductivity for the ceramic debris samples taken from the TMI-2 lower plenum varied from 1.0 to 3.8 W/mK over a temperature range from 1000 to 1800 K. The sample-to-sample variation at 1800 K was approximately 1.7 to 3.8 W/mK.[6] Please correct discrepancies between Appendix L and Table 7.1 material property values and revise calculations to consider appropriate values and uncertainties.

480.451 SCDAP/RELAP5 data[7] suggest that thermal properties for stainless steel (specific heat and thermal conductivity) differ from the iron properties assumed in Appendix L and Table 7.1 for the stainless steel in the metal layer. For example, the conductivity of stainless steel at 1700 K appears to be closer to 36 W/m-K than the 25 W/m-K value cited in Table 7.1. Why weren't stainless steel properties used in these calculations and what impact would the appropriate properties have on the results?

Decay Heat Assumptions

480.452 The total decay power shown in Figure 7.1 appears reasonable compared to SCDAP/RELAP5 calculations, which agree with the ANS 5.1 Standard. However, the ANS Standard includes estimates of uncertainty, which should be considered. For example, if one assumes knowledge of the core power within ~2% and knowledge of each of the ^{235}U, ^{238}U, and ^{239}Pu power fractions within ~1%, the Standard indicates a 1 σ uncertainty in decay power of ~5%. In order to capture ~95% of the uncertainty in decay power for those assumptions, one would need to place error bands of ± 10% (± 2 σ) on the decay power curve in Figure 7.1. In order to conclude that thermally-induced failure of an externally flooded, AP600-like reactor vessel is "physically unreasonable," more than a 2 σ uncertainty should be considered. Please assess the impact of decay heat uncertainty.

480.453 Discussion on p. 7-9 indicates that the most likely time for core relocation lies between 4 and 5 hours with a supporting reference to a MAAP calculation. However, SCDAP/RELAP5 calculations indicate relocation begins at 3 hours. A recently completed, revised MAAP calculation[8] also indicates a much earlier challenge to the lower head, with the beginning of relocation to the lower plenum shortly after 2 hours, and depletion of water in the lower head at approximately 2.7 hours. Please quantify the impact of earlier relocation times on your results by shifting the distribution of Figure 7.7 by 2 hours.

480.454 Results from SCDAP/RELAP5 calculations indicate an initial molten pool power density of ~1.5 MW/m^3. This value is conservative relative to the treatment given in the subject report because uniform mixing of molten pool components is assumed in SCDAP/RELAP5. Specifically, if one assumed metallic segregation (as is done in DOE/ID-10460), the power density would increase to an initial value of ~1.7 MW/m^3. On that basis, it would seem that the maximum value of 1.4 MW/m^3 given in Figure 7.8 is too low. Please consider a distribution that accommodates the possibility of these higher power levels.

Assumed "Bounding" End State Condition

480.455 As noted by Levy and a number of the reviewers, the assumed end state condition shown in Figure 2.2 is not necessarily the bounding or even most plausible configuration for the stratification of frozen and molten material. Figure 7 illustrates several possible asymmetric, idealized configurations that may be more challenging than the one assumed in Reference 1.

Configuration A corresponds to results from SCDAP/RELAP5 calculations for a similar scenario. (This calculation is not yet complete in that a further assessment of lower head heat transfer and the potential for additional relocation of steel is still to be completed). The configuration is characterized by a large oxidic pool (~85% of the core inventory) with a small metallic component (~5600 kg of unoxidized Zr and ~3400 kg of stainless steel). This configuration developed primarily as a result of localized relocations through the reflector sidewall. The stainless steel component accumulated from the melting of gray rods and the addition of lower plenum structures that melted as a result of being submerged by the debris. Calculations suggest that this configuration could persist for a period of time necessary to completely boil water in the lower head and then melt portions of the lower core plate. During this period, the metallic layer of ~10 cm would remain well below the threshold of 15 cm, which was given as the thickness necessary to insure vessel integrity under 'focused' heat loads. Furthermore, asymmetries ***could*** be expected in the core region as a result of the break location and the conditions that could develop in the vicinity of other major vessel penetrations (e.g., accumulator flow lines, core makeup line). These asymmetries that could significantly reduce steel melting and, ultimately, the thickness of the 'focusing' layer. In the main results, please assess the impact of a thin-metallic layer on lower head integrity, as a result of potential relocation scenarios and as a result of acknowledging asymmetries in core melt progression.

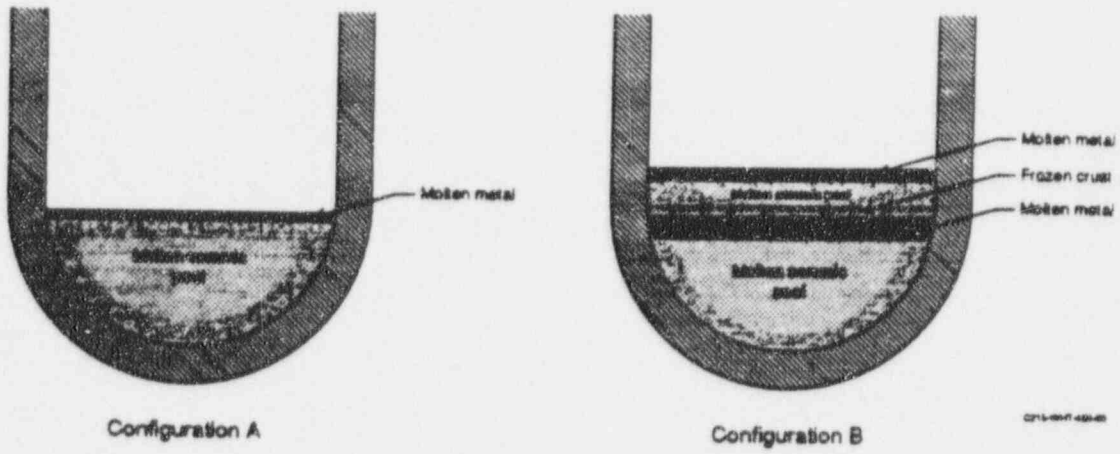

Figure 7. Possible endstates that may be more challenging than the Reference 1 endstate.

In Configuration B, a second pour would relocate onto the core plate forming a crust above the core plate. Any subsequent pours result in a second molten pool with a thin metal layer above it. As discussed above, multiple pours are possible because there are non-axisymmetric heat transfer boundaries. The core plate would be heated from below by the molten pool and above by the overlying crust. Metal in the core plate would become molten and eventually superheated, possibly resulting in a more severe heat load to the vessel than that postulated in the report. Hence, the idealized configuration shown in Figure 2.2 is only one of many plausible configurations. As discussed in Appendix O, factors such as the "random nature of boiling crisis (as found in ULPU), natural asymmetries in the thermal loading," etc. will make it highly unlikely that the actual endstate in the lower head is axisymmetric. Hence, there are a number of additional scenarios that could have been considered that may be more plausible than the configuration presented in Figure 2.2. As Dr. Levy noted, if the molten stainless steel becomes trapped below a crust of ceramic material, the molten stainless steel must either continue to heatup above the melting point of the ceramic crust or mechanically break through the crust to migrate to the top of the ceramic layers. In the event that molten steel becomes trapped below a crust of ceramic material, please assess the thermal loads on the vessel and the margin to vessel failure in the steel region.

480.456 The calculated upper surface temperatures in the metallic layer, Figure Q.8, and inner temperatures for the upper core barrel temperatures, Figure Q.10, are well below the melting point of stainless steel. What mechanism caused the upper stainless steel structures to melt and produce the quantity of molten metal assumed in Figures 2.2 and 7.5?

480.457 The metallic layer shown above the oxidic pool in Figure 5.1 is a basic assumption of the analysis outlined in this report. Is there evidence to show that this segregation will develop and persist in a turbulent natural circulation environment? This point is noted as an open issue by Dr. Turland (item 7). Are there conditions where lower head integrity could be adversely impacted if this segregation does not develop? If segregation occurs, could other configurations (i.e., a thin layer of absorber materials) adversely impact vessel integrity?

Heat Addition Due to Chemical Interactions

480.458 Section 7 calculations omit heat addition due to the metallic layer oxidation. As discussed by Professor Olander, ignoring the heat generation associated with the oxidation of the metallic materi-

als in the core is not only non-conservative, but clearly is at odds with the behavior that has been demonstrated in numerous experiments with prototypic materials. Professor Olander also noted that the metallic layer will oxidize quickly in the presence of steam and even more quickly in air. Although Professor Olander's comments were specific to the oxidation of zircaloy present in the metal layer, stainless steel will also oxidize rapidly in steam and air.

While the heat of reaction for stainless steel is less, 270-650 kJ/mole (depending on the final products formed), than that of zircaloy, 1200 kJ/mole, oxidation of stainless steel is important for several reasons. First, if it cannot be shown that the total oxidation rate is limited by the availability of steam and air, the total heat addition considering both stainless steel and zircaloy is significantly more than for zircaloy alone. Second, the reaction rates for stainless steel and zircaloy are comparable at or near the melting point of stainless steel. In fact, the reaction rate data from several investigators, including Bittel, Wilson, Leistikow, and Baker,[9 through 14] show that the oxidation rate for stainless steel exceeds that of zircaloy as the melting point of stainless steel is reached. Third, the oxidation of stainless steel results in swelling and foaming of the material as melting temperatures are reached. This results in highly porous debris in regions where the stainless steel mixes with the fuel and zircaloy. For example, in many of the integral bundle heating and melting experiments conducted at low pressure in CORA and ACRR, the frozen U-Zr-O in regions where stainless steel structures were present exhibited a froth-like appearance, resulting in a density of the U-Zr-O substantially lower than UO_2 or ZrO_2. Conduction through this porous region provides some insulating material on top of the metal layer, enhancing heat transfer to the side walls. Once oxidation is complete, the oxidized metallic layer provides additional insulation above the ceramic debris and increase downward heat loads to the vessel. Fourth, the presence of small amounts of iron oxides in debris composed primarily of $(U,Zr)O_2$ can significantly impact the properties of $(U,Zr)O_2$. For example, thermal diffusivity measurements of TMI-2 ceramic debris varied as much as ±50%. As noted by Uetsuka,[6] the most influential factor in that variation was the presence of a second phase composed of ferrous oxide.

In their response to Olander, the authors noted that oxidation of the metal layer could be neglected because (a) there would not be sufficient steam present to allow the reaction to proceed at the rate noted by Olander ("any containing supply of steam, as assumed, has to come from the containment atmosphere, together with lots of *air*") and (b) the increase in emissivity of 0.8 would more than compensate for additional heat generation. However, as Olander pointed out, the addition of air dramatically increases oxidation of steel and zircaloy due to the large increase in the heat of reaction.

480.458 a) Was the water initially present in the lower head during relocation considered as a source for oxidation?

b) Please document the mass flow rates of steam and air into the vessel and demonstrate that oxidation of metals in the core would be prohibited during later stages of the accident.

c) Please quantify the effects of the energy possible from stainless steel and zirconium oxidation, the reduced upward losses from a metallic layer with an oxidized upper surface, and the increased focussing associated with a thinner, unoxidized metallic layer.

Radiative Boundary Condition on the Upper Surface of the Melt

480.459 The radiative heat transfer model for the debris upper surface assumes an idealized set of conditions that maximize heat transfer from that surface. In one instance, it appears that this model was applied to a configuration that violate modeling assumptions. It is noted in the report that the radiation exchange between the upper surface of the melt is dominated by the temperature at the melt surface since (a) the radiation from the remaining structures is small because of the large surface area relative to the melt surface and (b) the radiation from the steam/air/aerosol atmosphere can be neglected because the atmosphere was transparent and any aerosols had been

previously deposited on colder surfaces. In addition, the detailed model assumes a very idealized geometry with a plate of a single thickness between the melt surface and the vessel wall. This may or may not be appropriate depending on the actual geometry of the structures remaining above the molten pool. For example, in the extreme parametric case it appears that this model was used under conditions where the assumptions would not be valid. In this case, where the molten metallic layer was in contact with the lower support plate, a relatively small fraction of the molten metallic layer would be able to see the colder vessel structures. Thus the radiative sink temperature, $T_{s,o}$, of approximately 920 K (Figure Q.10) and the melt surface temperature, $T_{s,i}$, of approximately 960 K would be inappropriate for such a configuration.

480.459 a) What calculations have been performed to insure that the absorption and emittance by the atmosphere in the vessel can be neglected, particularly if aerosols are being released from the surface of the metallic layer?

b) What calculations have been performed to verify that the aerosol generation and deposition rates for the conditions represented by Figure 2.2 would result in the absence of aerosols in the vessel atmosphere? If available, please provide supporting MAAP results concerning the atmosphere above the pool.

c) A very idealized geometry was assumed for the radiation heat transfer. What thicknesses, δ_s and δ_o, and surface area, S_s, were used in the calculations presented in Chapter 7 for the Figure 2.2 scenario and the "extreme parametric study"?

Structural Analyses

480.460 The objective of Section 4 is to demonstrate that structural failure won't occur in cases where the vessel wall is reduced to critical heat flux limited thicknesses. The following logic was applied by Theofanous et al. to prove that vessel failure will not be governed by structural failure.

- Section 4.1 establishes the required thickness to support dead loads (no thermal stresses) when the vessel is at full strength. In this section, it is concluded that the required thickness is 0.15 mm.
- Section 4.2 should demonstrate that after thermal stresses are considered, the vessel still has the capacity to support the dead loads. It states that the load carrying capacity is governed by the wall thickness that is under tension and that this thickness is approximately 5 mm.
- Though never directly stated, the reader is supposed to compare the 0.15 mm of required wall thickness to the 5 mm of wall under tension and conclude that the vessel can easily carry the dead load.

The structural analysis considers the vessel as a thin-walled hemispherical shell. The vessel is assumed to be completely depressurized, so only dead loads and buoyancy forces are considered. The vessel is also assumed to have a linear temperature distribution through its thickness, with an outside wall temperature of 400 K and an inside temperature of 1573 K. The upper temperature is based on the liquidus temperature of a specific iron/zircaloy eutectic composition.

An approximation to a closed form solution for thermal stresses in a cylinder (Equation 4.1), away from end conditions, was use to determine the distribution of stress in the ablated section of the vessel wall at the melt pool's metallic layer interface. This development neglected the radial stress component which has a lower maximum magnitudes throughout the wall thickness than the azimuthal or axial components of stress. INEL calculations of the radial stress, calculated elastically, indicate radial stresses of about 10 MPa compared to the elastic tangential stresses of around 1500 MPa. These tangential stresses will be limited to the yield stress at temperature, which is about 250 MPa (See Fig. 4.6) in the segment of the vessel wall expected to carry the dead loads. Therefore, neglecting the radial stress is appropriate. With that assumption,

Section 4 indicates that there is an inner region of the vessel wall that remains elastic and is available, with the outer segment in the vessel wall that is in tension and slightly yielded due to thermal stress, for some additional load-carrying capacity to withstand the net gravity force of the core melt after the buoyancy force of the water in the flooded reactor cavity is considered. If one assumes elastic-perfectly-plastic material, there can be no additional tensile load-carrying capacity in the material previously tension-yielded. So the load capacity margin of the vessel discussed in Chapter 4 is not nearly as high as is inferred.

A more rigorous indication of structural capacity of the ablated section was demonstrated by the elastic-perfectly plastic thermal structural analysis performed using a finite element approach in the Addendum to Chapter 4. This additional analysis was meant to answer reviewer concerns for ductile tearing and answered several concerns left open in the original development. This analysis apparently did not include creep effects but did give a good idea of how thermal stress would redistribute and confirmed the existence of an inner segment of the vessel wall that could be called upon for longer term dead weight loading capacity of the vessel wall. There was no detail on the boundary conditions, mechanical loading, or mechanical properties used and one is left to assume that these have been appropriately modelled for the problem at hand.

Approximate Solution

480.460 a) The approximate Equation 4.1 is meant to determine stresses in a cylinder's wall well away from its end conditions. What is the effect of end conditions (the vessel head below and the thicker cylinder wall above) on the stresses calculated in the ablated area?

b) The stress goes up more than 10 fold for a system pressure differential of 1.5 MPa. Table 7.4 indicates that IVR may be use as a mitigation scheme for cases 1APC and 3DC which are partially depressurized conditions. Given that IVR is to be considered for such conditions, please discuss the margin in the vessel for cases with low pressure.

c) On page 4-3, Theofanous et al. state:

"Thus the load carrying capacity of the vessel will be governed by the outer thickness of the wall that is under tension. Below, we will show that for the conditions of this problem, this outer region has a thickness of about one-fifth the wall thickness; that is ~5 mm thick for the limiting case considered in Figure 4.2."

The load carrying capacity of the vessel is not governed by the outer wall under tension. In a hanging vessel, such as this one, dead loads create tensile stresses. Given that an elastic-perfectly plastic assumption was assumed in the analysis and that the thermal stresses have plastically yielded the outer tensile region, the load carrying capacity for dead loads is governed by the portion of wall which has not yielded in tension (the inner four-fifths). Referring to Figure 4.6, most of the outer one-fifth wall has yielded in tension and is not available to carry more tension.

d) SA508 and SA533B1, two typically used pressure vessel steels, have structural properties that are quite similar. However, SA106B has considerably different properties at higher temperatures. Neither SA106B nor SA533B1 maintain full strength (355 MPA) up to 900 K. At 900 K, the yield strength for SA106B drops to 133 MPa[15] and SA533B1 drops to about 200 MPa.[16] Why was the full yield strength used in this strength determination? The lower actual yield stresses at temperature reduce the vessel's capacity accordingly. Please demonstrate that the AP600 steel properties are closer to the properties of SA106B than SA533B1 as stated on Page 4-4.

e) The reader is referred to an unspecified place in Section 7 to see the basis for the liquidus temperature, although the phase diagram is actually found in Figure 6.1. Note that Figure 6.1 shows that the liquidus temperature for this eutectic composition may vary by several hun-

dreds of degrees. However, Section 4 only indicates that one temperature was considered. As discussed above, if the range of possible temperatures were considered along with other uncertainties in predicting the wall thickness, the range of wall thicknesses shown in Figure 6 are possible. Please revise this analysis assuming an appropriate minimum wall thickness.

480.460 f) This analysis claims all of the unyielded inner-wall region and the outer plastically stressed region due to the accident thermal loads can be applied to the vessel's ultimate capacity to hold the dead weight loads. While there is some indication that the vessel might withstand these loads, this calculation alone does not adequately prove that, and margins of safety are not clear from the analysis in the original part of Chapter 4.

Finite Element Analysis

g) The finite element analysis was not well defined. What were the mechanical boundary conditions of the vessel finite element model? What was the mechanical load applied? What mechanical properties were used? What were the inner surface wall temperatures above the 72 degree location shown in Fig. 4.7?

h) The original content of Chapter 4 (Page. 4-6) refers to Appendix G of the report for a supporting argument that creep will not substantially change the result. Appendix G discusses a creep analysis of a vessel with internal pressure of 400 psi and a 5 cm. thickness and was run for an accident time of 15 hours. While this analysis is interesting for general trends of stress redistribution in the vessel wall, it offers little guidance in determining margins to failure for the specific, ablated vessel wall case considered in Chapter 4.

i) In Figure 4.6, the authors present results of a finite element analysis which includes only thermal stresses. Were dead loads included in this finite element analysis? Figure 4.6 also indicates that the wall thickness is 2.5 cm; whereas Figures 4.1 and 4.2 shows that the wall thickness in the critical region (between 70 and 90 degrees) should be approximately 2.5 cm. As discussed above, INEL analyses indicate that the minimum wall thickness may be considerably lower. Please repeat this analysis considering dead loads and an appropriate minimum wall thickness.

j) The analysis of the Addendum to Chapter 4 is meant to address ductile tearing and calculates strains in the 7 to 18% range. Please quantify the strain levels that would be of concern. Please discuss if these strain levels are temperature-dependent.

k) A number of different structural failure scenarios have been discussed at INEL, such as vibratory loading (from bubble formation in the cavity) of the lower head under the degraded wall conditions, shear loads in the degraded wall due to unbalanced loading of debris bed and the buoyant force, and thermal shock effects on the vessel. Thermal shock was brought up by the reviewers, Professor Olander and Dr. Tuomisto, with a focus on the possibility of brittle behavior of the vessel wall during the fuel melt relocation onto the lower head. The outer vessel wall will actually undergo tensile stress conditions during two phases of the accident: (1) during cavity flooding in which the vessel wall outer surface temperature will drop at a rapid rate from about 550 K to 373 K with the vessel depressurizing from operating pressure to some nominally low pressure (0.5 MPa); and (2) later in time during the melt relocation to the lower head when only thermal stresses cause the tensile stress on the outer surface of the vessel. The author's response to the reviewers' questions is based on the future design specifications for the vessel material to provide material that can withstand an accidental flooding and an end of life RTNDT sufficient to ensure that the material will stay ductile. It is not clear whether the RTNDT discussed is low enough that the above phase (1) cannot shift the RTNDT to a higher temperature level under the thermal load rate of the condition to cause brittle behavior and possible crack initiation. If preliminary crack damage to

the outer segment of the vessel wall were to occur during phase (1), then the available tensile load capacity required in phase (2) would be diminished. Has thermal stress load rate been considered in the pressurized thermal shock of phase (1)?

480.460 1) The vessel material design RTNDT is given in degrees Fahrenheit on page 7-22 and in degrees Centigrade on page T- 77. Please clarify which scale is appropriate.

Typos/Errors

480.461 a) The Equation numbers in Figure 5.8 are incorrect.

b) The footnote for Figure 5.8 is missing (see responses to Dr. Seghal's Item 8 and Dr. Schmidt's Item 6).

c) Equation 5.12 should be Equation 5.22 in paragraph (b) on page 7-13.

d) The word, "lease" should be "least" in paragraph 2 on page B-4.

e) Figures E.20 and E.21 are switched.

f) The word, "fashion" is misspelled in item 3 on page O-16.

g) Figures V.1 and V.2 from Appendix V do **not** contain heat flux values estimated to have caused the hot spot and the captions for these figures are incorrect. These figures contain the average heat fluxes and vessel temperatures estimated when nominal and lower bound values from TMI-2 data (debris mass, composition, decay heat, etc.) were assumed. As noted in the Stickler reference, the global vessel temperatures estimates from either of these case were considerably higher than vessel temperatures inferred from the TMI-2 vessel steel samples. In fact, for the pressures occurring during the TMI-2 accident, these average vessel temperatures were sufficient to result in vessel failure. Hence, additional cooling, not currently considered in severe accident analysis models, must have occurred during the TMI-2 accident. Section 5 of the Stickler reference discusses calculations in which local heat fluxes were superimposed on the vessel in order to induce inner vessel temperatures corresponding to the hot spot temperatures inferred from the TMI-2 vessel steel samples (1400 K).

References

1. T. G. Theofanous, et. al., In-Vessel Coolability and Retention of a Core Melt, DOE/ID-10460, July 1995.

2. J. H. Min and F. A. Kulacki, *Steady and Transient Natural Convection with Volumetric Energy Sources in a Fluid Layer Bounded from Below by a Segment of a Sphere - Annual Report 6*, July 1976- September 1977, NUREG/CR-0006, February, 1976.

3. G. A. Greene, O. C. Jones Jr., C. E. Schwartz, and N. Abuaf, *Heat Removal Characteristics of Volume Heated Boiling Pools with Inclined Boundaries*, NUREG/CR-1357, BNL-NUREG-51157, 1980.

4. C. M. Allison, J. L. Rempe, and S. A. Chavez, *Design Report on SCDAP/RELAP5 Model Improvements - Debris Bed and Molten Pool Behavior*, INEL-94-0174, November 1994.

5. Personal conversation between J. Rempe, INEL, and T. Y. Chu, SNL, April 1996.

6. H. Uetsuka, "Thermal Property Measurement of TMI-2 Debris," *presented at SARJ-94, Tokyo, Japan*, November 1, 1994.

7. C. Allison, et. al., *SCDAP/RELAP5/MOD3.1 Code Manuals, Volume 4: MATPRO- A Library of Materials Properties for Light Water REactor Accident Analysis*, Idaho National Engineering Laboratory Report, NUREG/CR-6150, EGG-2720, June 1995.

8. Letter from Westinghouse to NRC, dated April 4, 1996.

9. J. T. Bittel, L. H. Sjodahl, and J. F. White, "Oxidation of 304L Stainless Steel by Steam and Air," *Corrosion 25*, pp. 7-14, 1969.

10. R. E. Wilson and C. Barnes, *Chemical Engineering Division Semiannual Reports*, January-June 1964, ANL-6900, August 1964, p. 239.

11. R. E. Wilson et al., *Chemical Engineering Division Semiannual Reports*, July-December 1965, ANL-7125, May 1966, p. 150.

12. R. E. Wilson et al. in "Chemical Engineering Division Semiannual Reports," July-December 1966, ANL-7325, April 1967, p. 136.

13. S. Leistikow, "Comparison of High-Temperature Steam Oxidation Kinetics Under LWR Accident Conditions: Zircaloy-4 Versus Austenitic Stainless Steel No 1.4970," *Proceedings of the Sixth International Symposium on Zirconium in the Nuclear Industry*, June 1984 pp. 763-778.

14. L. Baker, *An Assessment of Existing Data on Zirconium Oxidation under Hypothetical Accident Conditions in Light Water Reactors*, ANL/LWR/SAF 83-3.

15. J. L. Rempe, et al., *Light Water Reactor Lower Head Failure Analysis*, NUREG/CR-5642, EGG-2618, October 1993.

16. L. A. Stickler, et al., *Calculations to Estimate the Margin to Failure in the TMI-2 Vessel*, NUREG/CR-6196, TMI V(93)EG01, EGG-2733, March 1994.